# Wavelet-Processed Flight Data for Robust Aeroservoelastic Stability Margins

Marty Brenner* and Rick Lind†

*NASA Dryden Flight Research Center, Edwards, California 93523-0273*

**Wavelet analysis for filtering and system identification is used to improve the estimation of aeroservoelastic (ASE) stability margins. Computation of robust stability margins for stability boundary prediction depends on uncertainty descriptions derived from the test data for model validation. Nonideal test conditions, data acquisition errors, and signal processing algorithms cause uncertainty descriptions to be intrinsically conservative. The conservatism of the robust stability margins is reduced with parametric and nonparametric time-frequency analysis of flight data in the model validation process. Nonparametric wavelet processing of data is used to reduce the effects of external disturbances and unmodeled dynamics. Parametric estimates of modal stability are also extracted using the wavelet transform. F-18 High Alpha Research Vehicle ASE flight test data are used to demonstrate improved robust stability prediction by extension of the stability boundary from within the flight envelope to conditions sufficently beyond the actual flight regime. Stability within the flight envelope is confirmed by flight test. Practical aspects and guidelines for efficiency of these procedures are presented for on-line implementation.**

## Nomenclature

| | |
|---|---|
| $a, a_i$ | = wavelet scale, indexed scale values (dimensionless) |
| $F(P, \Delta)$ | = feedback interconnection structure |
| $g$ | = wavelet basis function |
| $K$ | = feedback control system |
| $P(s), \hat{P}(s)$ | = Laplace transform of system plant, estimate |
| $W_{add}, W_{in}, W_{ns}$ | = weightings on $\Delta_{add}, \Delta_{in}$, noise |
| $W_g$ | = continuous wavelet transform with basis $g$ |
| $X(\tau, \omega), \hat{X}(\tau, \omega)$ | = wavelet-transformed signal, filtered signal |
| $X(\omega), \hat{X}(\omega)$ | = frequency-domain signal, estimate |
| $x(t), \hat{x}(t)$ | = time-domain signal, filtered signal |
| $\Gamma$ | = robust stability margin |
| $\Delta, \hat{\Delta}$ | = uncertainty operator, estimate |
| $\delta_{\bar{q}}$ | = uncertainty in flight condition |
| $\zeta$ | = damping ratio |
| $\mu$ | = structured singular value |
| $\tau$ | = wavelet translation time |
| $\phi(t), \phi_0$ | = signal phase, constant phase lag |
| $\omega_d, \omega_n$ | = modal damped and natural frequency |
| $\omega_0$ | = wavelet peak frequency |

## I. Introduction

ENVELOPE expansion of new modified aircraft often requires structural stability testing to verify safety margins to prevent against aeroservoelastic (ASE) instability. In-flight testing allows determination of aeroelastic or ASE effects as a function of flight parameters. Flight data are acquired for stability estimation and system identification to compare with analytic predictions. Any anomalies are regarded with care for safety of flight. Improvement in flight data analysis is achieved by discriminating areas of low signal-to-noise ratio, unmodeled dynamics, and external disturbances.[1]

Wavelet transforms have been applied to parametric identification of time-varying multiple-degree-of-freedom systems by estimation of the impulse response using correlation methods.[2,3] Modal frequency and damping parameters are estimated directly from the data without intermediate model identification schemes. However, these estimates require parameter range approximations to discriminate modal frequency and damping.

Recent methods[4,5] use a wavelet transform (WT) on free-response data to directly supply information on time-dependent modal decay rate and phase variation. Without any approximation of parameter range, estimates of modal frequencies and damping ratios are extracted from the response. Damping and frequency trends are useful for noting changes in system dynamics as a function of flight condition, thereby helping to reduce conservatism in real parameter variations of the uncertainty model.

Wavelet signal processing has also shown promise for system identification by application as filter banks for data enhancement[6] with continuous WTs. Time-frequency nonlinear filtering procedures have utilized constant resolution, continuous wavelet basis functions to enhance transfer function estimation.[7,8] Constant resolution analysis in time and frequency is generally not appropriate for transient system dynamics, however, because features of the relevant dynamics at different scales are ignored. Multiresolution analysis advances this capability with the discrete wavelet transform (DWT) to decompose the data into multiple scales to reveal prominent and subtle features regardless of the governing dynamics.[9]

Adjustable time-frequency resolution techniques provide flexibility with a DWT to resolve system dynamics from general nonstationary, transient signals. The objective of adjusting the competing requirements of time and frequency resolution with fast, accurate processing is accomplished with a combination of compact orthogonal and harmonic wavelet properties.[10,11] This paper exploits the multiresolution analysis property of the DWT for filtering and modal estimation algorithms. Emphasis is on the application of multiresolution Morlet wavelets as a signal transformation for dynamics analysis beyond standard bandpass noise filtering properties.

Model validation is a critical procedure in the computation of robust stability margins. The margins are adversely affected by poor characterizations of the uncertainty size and structure. The major contribution of this paper is augmentation of a fast multiscale wavelet filtering algorithm[10,11] with wavelet-based modal parameter extraction[5] to estimate robust stability margins with reduced-norm uncertainty sets of both complex-nonparametric and real-parametric perturbations. The decrease in conservatism results in a more practical and valuable robust stability margin.

Transfer functions and modal parameter estimates derived from time-frequency Morlet wavelets are used to estimate state space ASE models from F-18 High Alpha Research Vehicle (HARV)[12] flight data. These models are used in a robust stability boundary prediction

*Aerospace Engineer, Aerostructures Branch, MS 4840D/RS. E-mail: martin.brenner@dfrc.nasa.gov.

†Aerospace Engineer, Aerostructures Branch, MS 4840D/RS. E-mail: rick.lind@dfrc.nasa.gov. Member AIAA.

method based on the structured singular value $\mu$ (Ref. 13). On-line implementation issues are presented to demonstrate feasibility in a flight-test environment.

## II.  ASE Flight Test

The HARV aircraft was a modified F-18 to include thrust vectoring paddles on the engines and a research flight control system to ensure stability at high-angle-of-attack flight conditions.[14] The flight system also included an excitation signal generator, designated as onboard excitation system (OBES), for aerodynamic parameter identification, closed-loop stability monitoring, and aeroservoelastic excitation.[15] For ASE stability monitoring, the OBES was configured to sum programmed digital signals to the control system actuator commands for structural excitation of the primary modes. Inputs from 5 to 20 Hz were added to the control surface commands for flight conditions with angles of attack from 5 to 70 deg.

Analytical predictions indicated poor ASE stability robustness in the lateral-directional feedback loops. Structured singular values of complementary sensitivity near the first antisymmetric wing bending and wing torsion modes (about 9 and 12 Hz, respectively) approached 0 dB, and the wing fore–aft mode near 15 Hz was at $-6$ dB. Flight envelope limits were 15,000–35,0000 ft altitude up to Mach 0.7. Worst-case flight conditions from the analysis were less than Mach 0.3, greater than 30,000-ft altitude, and above 50-deg angle of attack. This paper addresses robust stability at a representative worst-case flight condition of 50-deg angle of attack at Mach 0.3 and altitude 30,000 ft.

## III.  Time-Frequency System Identification

A desirable feature of signal analysis is adaptation to both transient and stationary characteristics, which implies both time- and frequency-domain resolution criteria subject to the uncertainty principle. These competing requirements demand a method that is tunable according to the local signal dynamics. For general types of input excitation, constant time-frequency resolution analysis[6,7] is too restrictive and generally not applicable. A multiresolution signal decomposition is, therefore, required.

Redundant continuous wavelet transform methods give arbitrarily good resolution, but are cumbersome[10] and often slow[16] for reconstruction and filtering. Alternatively, nonredundant (compact and orthonormal) wavelet transforms are fast and accurate, but are limited in frequency resolution even with wavelet packets. Good frequency resolution is obtained with classical harmonic wavelets,[17] but time resolution is sacrificed. Regulation of time and frequency resolution with fast, accurate processing is accomplished with a combination of compact orthogonal and harmonic wavelet properties in the compact harmonic wavelets.[10,11]

### A.  Nonparametric Estimation: Wavelet Filtering

The multivoice WT was introduced to exploit multiresolution analysis using compact harmonic wavelets.[10,18] Multivoice, or multiscale, refers to redundant representations of signals on multiple frequency bands.[19] Nonorthonormal Morlet wavelets are approximated with (harmonic-like) discretizations on multiple-wavelet scales. These form a nonorthogonal redundant basis for the signal space, which does not admit a multiresolution analysis. The derivation of a DWT from the wavelet basis is necessary to get a multiresolution analysis of the sampled continuous Morlet transform.[18]

The DWT is implemented as a filter bank covering a predefined range of frequencies with corresponding number of frequency bands (voices) per octave. Interpolation, or scaling, filters are introduced to define how the scales relate to each other in a dyadic fashion for the multiscale representation. These scaling filters are compact (finite impulse response) for fast and accurate reconstruction. Therefore, multivoice transforms provide practical, fast, and flexible means for analysis and filtering of nonstationary data with tunable frequency resolution vs time localization.

The WT of signal $x(t)$ over the timescale $(a, \tau)$ plane is represented as

$$W_g(a, \tau) = \frac{1}{\sqrt{a}} \int_{-\infty}^{\infty} x(t) g^* \left( \frac{t - \tau}{a} \right) \mathrm{d}t \qquad (1)$$

where scale parameter $a$ is proportional to the duration and inversely proportional to the peak frequency $\omega_0$ of the complex Morlet wavelet

$$g(t) = \left( 1 \big/ \sqrt{2\pi} \right) \exp(-t^2/2) \exp(i\omega_0 t) \qquad (2)$$

The spectrum of a dilated and translated Morlet wavelet reaches a maximum value at $\omega = \omega_0/a$:

$$G_{a,\tau}(\omega) = \exp\left[ -(a\omega - \omega_0)^2 \right] \qquad (3)$$

Multiscale data decomposition is performed by projection of the signal onto the wavelet bases of different scales. A timescale representation of the projection coefficients is often called a scalogram,[20] which is the power spectral density $|W_g(a, \tau)|^2$ of the signal over the $(a, \tau)$ plane. Time-frequency masking of input and output is performed in the $(a, \tau)$ plane, and the reconstruction into the time domain results in the filtered response. This is an extension of previous wavelet filtering procedures[6–8] because the time-frequency resolutions are adjusted for optimum performance.

An example scalogram of an F-18 HARV 5–20 Hz lateral acceleration feedback response from an aileron frequency sweep input is shown in Fig. 1. The filtering procedure on the output is shown in Fig. 1b as a processed scalogram. Figure 2 shows the effect of filtering on the time response.

### B.  Parametric Modal Estimation: Morlet WT

Modal parameters can be estimated with wavelets by analysis of the system impulse response[5,21] (see Appendix). The DWT of a signal using the complex Morlet wavelet is a complex-valued matrix, whose modulus and phase are related to impulse response parameters. In the current application, this procedure is applied at every time point assuming at each instant that the response is a sum of multiple-degree-of-freedom impulse responses.
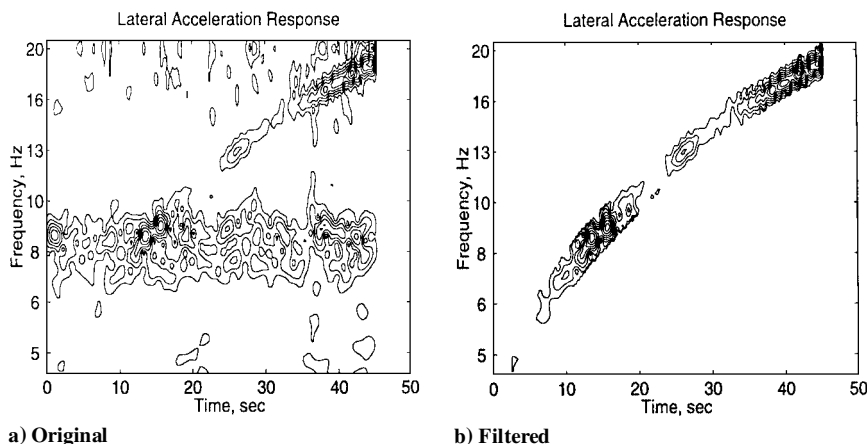


a) Original          b) Filtered

Fig. 1    Scalogram contours of lateral acceleration feedback response from aileron command input.

**a) Original**

**b) Filtered**

Fig. 2  Responses of lateral acceleration feedback response from aileron command input.



**a) Response natural frequency**

**b) Damping ratio**

Fig. 3  Time-dependent modal parameter estimates.



Fig. 4  Wavelet coefficient absolute magnitudes as functions of estimated modal frequency and damping estimates.
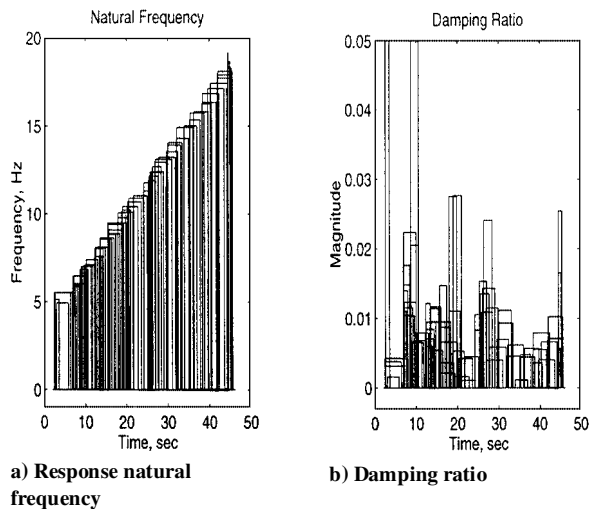
Data from the wavelet filtered results of Fig. 2 are used to estimate the mean value of the instantaneous frequency $\omega(t)$, or the estimated $\omega_d$, and the estimated decay rate $\zeta \omega_n$ as a function of the complex Morlet wavelet frequency $\omega_0$ (see Appendix). From these two parameters are derived the modal natural frequency $\omega_n$ and modal damping ratio $\zeta$ as functions of $\omega_0$. This bank of Morlet wavelets used for natural frequency and damping ratio estimation are time tagged for start and duration times to get the modal estimates as functions of time. Time-dependent modal parameter estimates are shown in Fig. 3. It is observed that modal frequency is essentially the tracked input frequency in this case because the cleaned output signal from Fig. 2b is being used, and this accelerometer response tends to track the input frequency. From the scalogram of Fig. 1b, the response lacks definition between 20–25 s and 32–34 s. These gaps also correspond to the lower output signal levels from Fig. 2b at these time intervals. Lack of observability adversely affects the modal estimates of Fig. 3 in these particular intervals.

Scalogram contours of Fig. 1 suggest the wavelet coefficients as a measure of data quality and modal definition. In Fig. 4 the wavelet coefficients are represented for each modal frequency and damping ratio using the same data from the wavelet filtered results of Fig. 2. Lower magnitude coefficients indicate less observable modal dynamics from the data. Coefficients from modal frequency estimates may be used to distinguish more dominant from less observable dynamics. This criteria can be exploited to extract the corresponding modal damping values.
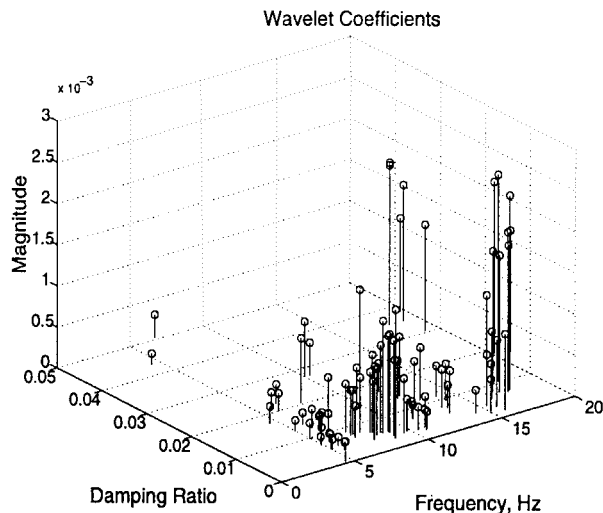
An important point is that the Morlet wavelets are being used to estimate the modal parameters; therefore, an implicit multiresolution filtering process is being performed independent of the explicit graphical procedure already described (Fig. 1). The wavelet basis representation of the signal is itself a noise-free subspace of the signal function space, and the modal parameters are derived from this signal subspace of wavelets with varying duration, frequency, and location in time.

## IV.  $\mu$  Method

A method to compute stability margins of aeroservoelastic systems has been formulated based on robust stability theory.[22] This method uses a set of structured operators $\Delta$, referred to as uncertainty, to describe errors and unmodeled dynamics in an analytical model. The structured singular value $\mu$ is used to compute a stability margin for this model that is robust, or worst case, to the uncertainty operators.[23]

The $\mu$ framework represents systems as operators with interconnections known as linear fractional transformations. This paper will use the notation $F(P, \Delta)$ to represent feedback interconnection of the plant $P$ and uncertainty $\Delta$. Aeroservoelastic systems may have errors affecting different dynamic subsystems so that the uncertainty operator $\Delta$ is structured such that the feedback interconnections ensure each subsystem is affected by the proper component of $\Delta$.

Flight data can be incorporated into the $\mu$ method by formulating an uncertainty description that accounts for observed variations and errors.[24] A model validation analysis is performed on the plant model to ensure the range of dynamics admitted by the uncertainty is sufficient to cover the range of dynamics observed with the flight data. Thus, a robust stability margin is computed that directly accounts for flight data.

An ASE stability margin $\Gamma$ is determined by computing $\mu$ with respect to an uncertainty description $\delta_{\bar{q}}$ that admits variations in dynamic pressure $\bar{q}$ and an uncertainty description $\Delta$ that describes modeling errors.[25] This margin relates the largest change in dynamic pressure that may be considered while guaranteeing the plant model is robustly stable to all errors described by $\Delta$.

## V.  $\mu$  Method with Wavelet Processing

The $\mu$ method can be coupled with the wavelet filtering processes of parametric and nonparametric estimation discussed earlier. This coupling is achieved by introducing several time-frequency operations based on wavelet filtering into the basic process. Figure 5 shows the general information flowchart for the $\mu$ method with wavelet filtering.

WT operations introduced earlier are used to process time-domain data $x(t)$ before a frequency-domain representation $\hat{X}(\omega)$ is computed. These operations map the time-domain data into a time–frequency domain scalogram via a WT and then map a scalogram back into the time domain via an inverse WT. A time–frequency
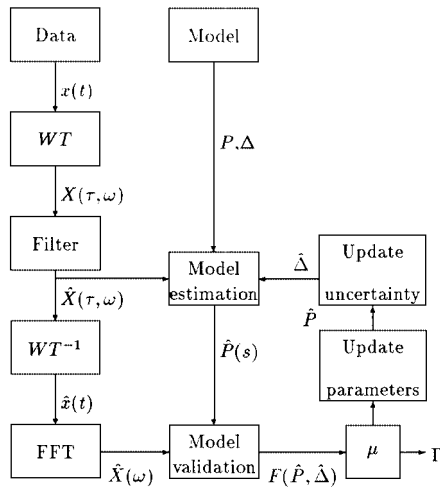
**Fig. 5   Flowchart of $\mu$ method combined with wavelet processing for on-line wavelet-$\mu$ method of robust stability margin analysis of ASE dynamics.**

filtering process operates between the WT and inverse WT to remove unwanted features from the scalogram before the inverse WT computes a time-domain signal, $\hat{x}(t)$.

A modal parameter estimation operation is introduced using the wavelet algorithm. Properties of the system dynamics are derived from the filtered scalogram. The elements of a nominal plant model $P$ are updated with these parameter estimates, and a new plant model $\hat{P}$ is used to represent the aeroservoelastic dynamics.

The final operations of the $\mu$ method are traditional robust stability operations that operate on frequency-domain data. The effect of the wavelet filtering is to use the filtered versions of the data and plant model for the modal validation. Thus, a new uncertainty operator $\hat{\Delta}$ is associated with the parameter updated plant $\hat{P}$ to account for errors observed from the filtered data $\hat{x}(t)$. A robust stability margin $\Gamma$ is computed that describes the largest change in dynamic pressure for which $\hat{P}$ is robustly stable to the errors $\hat{\Delta}$.

### A.   $\mu$ Method with Parameter Estimation

An implementation of the $\mu$ method with modal parameter estimation is accomplished using the flowchart of Fig. 5. The filter operation for this implementation is presently ignored, so that the wavelet map $\hat{X}(\tau, \omega)$ is equivalent to the original map $X(\tau, \omega)$.

The wavelet-based method for parametric estimation is used to analyze the wavelet map $\hat{X}(\tau, \omega)$ of the flight data. This method estimates modal parameters to describe the system dynamics that generated the flight data. A plant model $\hat{P}_1$ is computed by updating elements of the nominal plant model $P_0$ with the modal parameter estimates. Only a limited subset of dynamics will be observable in the data from the wavelet coefficients, and so only a correspondingly limited subset of the plant modal parameters will be updated.

An uncertainty description $\hat{\Delta}_1$ is generated for the plant with updated modal parameters $\hat{P}_1$ using the model validation procedure. This procedure essentially uses the original flight data measurements because the WT and inverse WT operations will cancel each other except for numerical inaccuracies. Thus, $x(t) \approx \hat{x}(t)$, and an uncertainty description is computed for the updated plant, which accounts for all variations and anomalies in the recorded data.

The magnitude of uncertainty associated with the updated plant should be less than (or equal to) the uncertainty magnitude associated with the nominal plant. This decrease in uncertainty results from the ability of the updated plant to account for bias in the nominal plant estimates. Hence, the uncertainty associated with the updated parameter is less than the uncertainty associated with the nominal parameter. Thus, $\|\hat{\Delta}_1\|_\infty \leq \|\Delta_0\|_\infty$.

The conservatism in robust stability margins computed by the $\mu$ method arises from the excessive uncertainty needed to account for errors in a model. A decrease in uncertainty from model updating with the parameter estimation process should decrease this conservatism.

### B.   $\mu$ Method with Wavelet Filtering and Parameter Estimation

Another implementation of the $\mu$ method with modal parameter estimation results from including a nontrivial filtering operation in the flowchart of Fig. 5. The wavelet filtering operation, which is a type of nonparametric estimation, is used to generate scalograms to represent desired features of input and output data in the time–frequency domain. The filtered scalogram $\hat{X}(\tau, \omega)$ may be arbitrarily different than the original scalogram $X(\tau, \omega)$, depending on the energy of the signal components that do not correlate to desired features.

The filtered wavelet map is input to the parametric estimation process. Resulting modal parameter estimates represent the dynamics of the system model that generates the desired features dominant in the filtered maps. The elements of the nominal plant model $P_0$ are replaced with the modal parameter estimates to generate an updated plant model $\hat{P}_2$.

The filtered wavelet map is also used to generate an uncertainty description for the updated plant $\hat{P}_2$. A time-domain signal $\hat{x}(t)$, which represents the filtered measurement data, is computed by an inverse WT on the filtered scalogram. A frequency-domain representation of this filtered signal is computed from a Fourier transform and is used by the model validation process. The resulting uncertainty $\hat{\Delta}_2$ describes the variations between the updated plant $\hat{P}_2$ and the filtered data.

The uncertainty description associated with $\hat{P}_2$ should be less (or equal) when validating the filtered data compared to validating the unfiltered data. The filtering process should remove nonlinearities and harmonics along with noise that causes aliasing and errors in measured transfer functions. This removal of errors may decrease the variance in modal parameter estimates so that an updated model can be generated with less uncertainty. The filtered data generate parameters that are less scattered allowing the uncertainty ball to be smaller, so that $\|\hat{\Delta}_2\|_\infty \leq \|\hat{\Delta}_1\|_\infty \leq \|\Delta_0\|_\infty$. Therefore, the conservatism in robust stability margins computed by the $\mu$ method may be decreased by including the wavelet filtering into the process.

## VI.   Aircraft Models and Uncertainties

Robust stability margins for the aeroservoelastic dynamics of the F-18 HARV are computed using the $\mu$ method with wavelet filtering. Stability margins are computed for the antisymmetric modes of the lateral-direction aeroservoelastic dynamics for the aircraft at Mach 0.3 and an altitude of 30,000 ft ($\bar{q} = 41$ lb/ft$^2$) at 50-deg angle of attack. A baseline implementation of the $\mu$ method indicates these margins may lie within the flight envelope so any reduction in conservatism could be significant at this flight condition.[22]

An uncertainty description is formulated using three operators to describe errors in an F-18 HARV analytical model. A complex operator $\Delta_{in}$ is a multiplicative uncertainty in the control inputs to the plant and accounts for actuator errors and unmodeled dynamics. Another complex operator $\Delta_{add}$ relates the control inputs to the feedback measurements to account for uncertainty in the magnitude and phase of the computed plant responses. The remaining uncertainty operator $\Delta_A$ is a real parametric uncertainty affecting the modal parameters of the open-loop state matrix to describe errors in natural frequency and damping parameters.
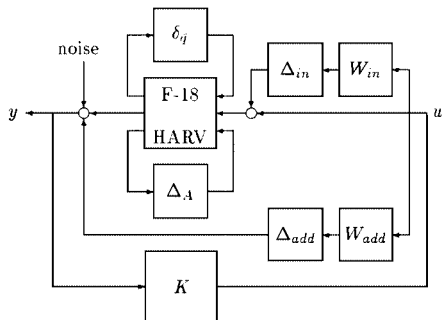
The block diagram for robust stability analysis of the F-18 HARV aeroservoelastic dynamics is shown in Fig. 6. This figure includes an operator $\delta_{\bar{q}}$ that affects the nominal dynamics to describe changes in flight condition and is used to interpret $\mu$ as a stability margin.[25] Additional operators $W_{add}$ and $W_{in}$ are shown as weightings to normalize the frequency varying uncertainty operators $\Delta_{add}$ and $\Delta_{in}$. The system model also contains 2% sensor noise corruption on each measurement. The lateral-directional controller $K$ has 29 states. There are four feedback measurements (roll rate, yaw rate, lateral acceleration, and sideslip rate) and six control inputs (aileron, rudder, yaw thrust vectoring, and differential leading-edge flaps, trailing-edge flaps, and stabilators) associated with this controller.

### A.   Baseline Model Validation

A model with an associated uncertainty description is generated to compute robust stability margins by the $\mu$ method. The plant model $P_0$ is the nominal model generated by a finite element analysis[15]

**Table 1    Modal parameters and uncertainty variations for model $P_0$ and $\Delta_0$**

| Mode | $\omega$, Hz | $\zeta$ |
|---|---|---|
| Fuselage first bending | $6.85 \pm 0.07$ | $0.012 \pm 0.006$ |
| Wing first bending | $8.96 \pm 0.18$ | $0.006 \pm 0.004$ |
| Wing first torsion | $12.84 \pm 0.13$ | $0.011 \pm 0.006$ |
| Wing fore–aft | $15.69 \pm 0.63$ | $0.010 \pm 0.007$ |
| Fuselage first torsion | $18.86 \pm 0.76$ | $0.010 \pm 0.005$ |

**Table 2    Modal parameters and uncertainty variations for model $P_1$ and $\Delta_1$**

| Mode | $\omega$, Hz | $\zeta$ |
|---|---|---|
| Fuselage first bending | $6.85 \pm 0.07$ | $0.012 \pm 0.006$ |
| Wing first bending | $8.60 \pm 0.10$ | $0.040 \pm 0.021$ |
| Wing first torsion | $13.31 \pm 0.15$ | $0.045 \pm 0.024$ |
| Wing fore–aft | $16.51 \pm 0.35$ | $0.045 \pm 0.023$ |
| Fuselage first torsion | $18.21 \pm 0.37$ | $0.030 \pm 0.010$ |

**Table 3    Modal parameters and uncertainty variations for model $P_2$ and $\Delta_2$**

| Mode | $\omega$, Hz | $\zeta$ |
|---|---|---|
| Fuselage first bending | $6.85 \pm 0.07$ | $0.012 \pm 0.001$ |
| Wing first bending | $8.70 \pm 0.09$ | $0.035 \pm 0.003$ |
| Wing first torsion | $13.31 \pm 0.14$ | $0.045 \pm 0.004$ |
| Wing fore–aft | $16.61 \pm 0.17$ | $0.045 \pm 0.004$ |
| Fuselage first torsion | $18.21 \pm 0.18$ | $0.040 \pm 0.004$ |



**Fig. 6    F-18 HARV uncertainty block diagram for robust stability margin analysis.**

of the aeroservoelastic dynamics. The parameters in this model are theoretical and have not been updated by analysis of flight data. The model contains seven antisymmetric elastic structural modes between 5 and 20 Hz.

An uncertainty description $\Delta_0$ is generated using the model validation procedure on a frequency-domain representation of the unfiltered data, $\hat{X}(\omega) = X(\omega)$. Only the observed energies from frequencies below 20 Hz are used for validation because there is considerable energy at frequencies near 20 Hz caused by structural dynamics associated with the thrust-vectoring vane system that are difficult to model. The primary transfer function used in the derivation of the uncertainty description is the lateral acceleration response from yaw thrust vectoring. These data responses demonstrate good observability of the primary modes up to 20 Hz based on spectral data.

Separate parametric uncertainty levels are determined for each mode of the open-loop state matrix to reflect different levels of accuracy. These uncertainty magnitudes describe observed variations between the model transfer function and the flight data measurements based on spectral model validation criteria.[13,24] All subsequent model validation tests use similar criteria. Table 1 shows the nominal modal parameters and the amount of variation admitted by the parametric uncertainty.

The amount of variation needed to describe modal parameter errors is fairly significant for all modes, especially in damping ratio. The fuselage first torsion and wing fore–aft modes have properties that are particularly poorly modeled and so there is up to 4% error in natural frequency and 70% error in damping. The remaining modes have only 2% error in natural frequency but still require at least 50% error in damping.

The weighting functions for the input multiplicative and additive uncertainties are chosen to account for any errors between the model and the flight data that can not be covered by the parametric modal uncertainty:

$$W_{\text{in}} = 10 \frac{s + 100}{s + 5000} \qquad (4)$$

$$W_{\text{add}} = 0.02 \qquad (5)$$

### B.    Model Validation with Parameter Estimation

The parametric modal estimation procedure is used to process the flight data and compute modal parameters for an analytical model. This procedure uses $W(a, \tau)$ to generate estimates of the modal parameters from the unfiltered wavelet map $X(\tau, \omega)$ and its properties.

A plant model $\hat{P}_1$ is computed, which is the estimated plant model obtained from the modal estimates. This model is formulated as an update of the nominal plant $P_0$ with modal parameters replaced by their estimated values. The nominal values of these parameters are

shown in Table 2. The natural frequencies are not changed by more than 1 Hz for any of the estimated modes; however, the estimated damping parameters are significantly higher than the theoretical values of Table 1.

An uncertainty description $\hat{\Delta}_1$ is associated with $\hat{P}_1$ to describe the levels of modeling error in this estimated plant. The magnitudes of the parametric modal uncertainty in $\hat{\Delta}_1$ are determined by comparing flight data with transfer functions for $\hat{P}_1$. The ranges of modal parameter variations admitted by this uncertainty are given in Table 2.

The variations in both natural frequency and dampings are seen to be considerably reduced for $F(\hat{P}_1, \hat{\Delta}_1)$ (Table 2) compared to the large variations for $F(P_0, \Delta_0)$ (Table 1). The estimated modal parameters used in $\hat{P}_1$ are much closer to those of the aircraft and so the response of $\hat{P}_1$ closely matches the flight data measurements. Thus, the natural frequency errors are all less than 2%, whereas the damping errors are all less than 55%. The weightings $W_{\text{add}}$ and $W_{\text{in}}$ affecting the remaining uncertainties in $\hat{\Delta}_1$ are identical to those of $\Delta_0$.

### C.    Model Validation with Wavelet Filtering and Parameter Estimation

Modal parameters for model estimate $\hat{P}_2$ are extracted from the time-frequency domain representation of the wavelet-filtered flight data $\hat{X}(\tau, \omega)$. This is the procedure outlined in Fig. 5. As shown in Table 3, the modal estimates from the filtered data are similar to the unfiltered estimates of Table 2. Parameter variations, however, resulting from validated model $F(\hat{P}_2, \hat{\Delta}_2)$ are reduced in modal frequency to 1% and in modal damping to 10%.

## VII.    Aeroservoelastic Stability Margins

Nominal stability margins are computed for the plant model using the original theoretical modal parameters and the updated models using parameters estimated from wavelet processing. These margins are computed from a $\mu$ analysis with respect to the variation in dynamic pressure $\bar{q}$, but ignoring the modal and complex uncertainty operators. The nominal stability margins $\Gamma$ (Table 4) demonstrate the largest decrease relative to the nominal dynamic pressure of $\bar{q} = 41$ lb/ft$^2$ that may be considered before the models incur an ASE instability. Therefore, a larger negative margin indicates a greater margin of robust stability.

The original theoretical model has a nominal stability margin of $\Gamma = -268$ lb/ft$^2$ resulting from a critical instability of the wing fore–aft mode at 14.8 Hz. The margins are increased by updating the models with modal parameters estimates; however, the wing fore–aft mode remains the critical mode for these updated models. This increase in stability margin associated with wavelet filtering is not guaranteed to occur for all applications; rather, the filtering is designed to increase nominal model accuracy. The nominal model for the F-18 HARV has excessively low damping values compared to the damping levels resulting from the wavelet filtering. Increasing damping ratio estimates makes the plant effectively more stable and increases the stability margins.

**Table 4  Nominal and robust stability margins**

| Nominal model | $\Gamma$, lb/ft$^2$ | $\omega$, Hz | Robust model | $\Gamma$, lb/ft$^2$ | $\omega$, Hz |
|---|---|---|---|---|---|
| $F(P_0, 0)$ | −268 | 14.8 | $F(P_0, \Delta_0)$ | −4 | 15.4 |
| $F(P_1, 0)$ | −368 | 14.8 | $F(P_1, \Delta_1)$ | −222 | 7.0 |
| $F(P_2, 0)$ | −379 | 14.8 | $F(P_2, \Delta_2)$ | −239 | 7.0 |

These nominal margins are all greater in absolute value than the nominal dynamic pressure and so they demonstrate the nearest instability to the flight envelope occurs at a negative dynamic pressure, which is physically unrealizable. Thus, the nominal dynamics are predicted to be free of ASE instabilities within the research flight envelope.

Robust stability margins are computed with respect to the uncertainty description of Fig. 6 and given in Table 4. Model $F(P_0, \Delta_0)$ describes the original model with parameter variations as in Table 1. The model with modal parameter estimates $F(P_1, \Delta_1)$ has the reduced uncertainty levels leading to the variations in Table 2. The remaining model $F(P_2, \Delta_2)$ describes the model formulated by combining wavelet filtering with parameter estimation and introducing uncertainty to allow the variations in Table 3.

The stability margin of the original model is strongly affected by considering uncertainty. This margin is reduced from $\Gamma = -268$ lb/ft$^2$ for the nominal dynamics to $\Gamma = -4$ lb/ft$^2$ for the dynamics with respect to uncertainty. The critical mode remains the wing fore–aft mode despite the uncertainty; however, the dynamic pressure at which this mode becomes unstable is quite different. This robust stability margin demonstrates the nominal model may be misleading and the nearest unstable flight condition may actually lie within the flight envelope. However, because the aircraft actually flew beyond the edges of the flight envelope without instability, this margin must be too conservative.

The robust stability margin for the model $F(P_1, \Delta_1)$, using modal parameter estimates, is significantly larger than the margin of the original system. The wavelet processing is able to identify a more accurate model with less associated uncertainty so that the conservatism in the margin is reduced. The robust stability margin for this model is $\Gamma = -222$ lb/ft$^2$ and indicates the nearest instability for the updated model. Despite the range of dynamics incurred by uncertainty, the margin is at a negative dynamic pressure, and so the flight envelope is now predicted to be free of ASE instabilities, as expected.

The critical mode associated with the robust stability margin for the updated model is the first fuselage bending mode. This differs from the critical wing fore–aft mode associated with the nominal margin. This shift in critical mode is a result of modal parameter updates and corresponding reduced uncertainty sets.

The model formulated from parameter estimation coupled with wavelet filtering $F(P_2, \Delta_2)$ has a robust stability margin that is similar to the margin of $F(P_1, \Delta_1)$. The magnitude of this margin is slightly higher as a result of the reduced uncertainty levels needed to validate the filtered flight data; however, the critical mode remains the fuselage bending mode.

Reduction in parameter variations from nonparametric wavelet filtering did not have as much an effect on robust stability as the updated parameter estimates. Nonparametric filtering has more impact on parameter variance, which was a less significant factor than parameter bias.

To summarize, comparison between the nominal results (Table 4) and the robust margins (Table 4) shows that the decrease in margin from uncertainty is clearly evident. The decrease is most substantial for plant model $P_0$, which has the greatest amount of modal uncertainty in $\Delta_0$, yet the frequency of instability is consistent with the nominal cases. When updated modal parameter estimates are incorporated in $P_1$ and $P_2$, the decrease in margins compared to the nominal models are somewhat less because of the smaller uncertainty sets ($\Delta_1$, $\Delta_2$) compared to $\Delta_0$.

The main difference between nominal and robust results is in modal frequency of instability. Wing fore–aft modal frequency increased about 1 Hz from its theoretical value to the updated value, and thereby became a less significant factor in the stability margin

calculation compared with first fuselage bending. This result confirms that the effect of parameter estimation, and essentially data quality, in model validation becomes a critical factor in robust stability boundary prediction.

## VIII.  On-Line Implementation

Analysis of flight data in an on-line environment requires interactive capabilities. In reference to the flowchart of Fig. 5, the data stream is first wavelet processed to provide information to the model validation step. Wavelet processing will require resolution criteria, filtering options, and a methodology for extracting dominant dynamics as from Fig. 4. A robust stability margin is then calculated based on the model validation test. Modal parameters can be incorporated into a model update, and uncertainty descriptions are modified accordingly. Finally, an updated model $\hat{P}(s)$ is created to close the loop until the next data stream is processed. A parallel effort of wavelet processing of future data while model updating from past data is, therefore, possible.

Model updates need to be performed in the context of the test scenario, flight conditions, and stability criteria.[13] Model parameters from more recent (local) tests can be used if stability prediction is based on a particular sequence of adjacent test conditions. This approach attempts to minimize conservatism for a particular area of the flight envelope or a particular flight regime. Alternatively, model uncertainty may be continuously increased in a worst-case approach to assure that all nominal models with the associated uncertainty description are not invalidated by any of the data sets. In this case, a single global uncertainty model is generated for conservative measures. A hybrid approach would segment areas of the flight envelope for a combination of local analyses in which each would have some flight condition commonality.

Computation requirements are reasonable. A 200-MHz computer is able to process multiple signals at multiple scales well within the time it takes to compute the model validation and $\mu$ step in a worst-case analysis for flutter prediction.[26] Hence, a complete on-line analysis for each test point during flight test is feasible within a couple minutes.

## IX.  Conclusions

Improvements in ASE flight data analysis and stability prediction estimation have been addressed. Wavelet approaches to system identification were applied by combining both filtering and parametric time–frequency identification algorithms with Morlet wavelets. The combination of these estimation schemes extracted modal estimates and system uncertainty representations for less conservative model validation. Uncertainty ranges determined by F-18 HARV aeroservoelastic flight test data were shown to decrease by incorporating modal estimates based on the wavelet-processed data.

With the model parameter and uncertainty description updates, the critical aeroservoelastic instability changed in modal frequency and flight condition. A predicted instability within the flight envelope using an uncertain baseline model was found to be too conservative, as confirmed by actual flight. Model updates pushed the instability beyond the flight regime. The ultimate objective of predicting stability boundaries from flight data was enhanced by a reduction in conservatism of the stability margin estimates.

## Appendix: Modal Parameters from the Morlet WT

Given a general harmonic signal

$$x(t) = k(t) \cos[\phi(t)] \tag{A1}$$

the WT of $x(t)$ is[5] $[\omega(t) = \phi'(t)$ is the derivative of the phase]

$$W(a, \tau) = \sqrt{a}k(\tau) \exp\left[-(a\omega(\tau) - \omega_0)^2\right] \exp[i\phi(\tau)] \tag{A2}$$

For fixed dilation parameter $a_i$, the modulus and phase angle ($\angle$) of the WT of $x(t)$ are

$$|W(a_i, \tau)| = \sqrt{a_i}k(\tau) \exp\left[-(a_i\omega(\tau) - \omega_0)^2\right] \tag{A3}$$

$$\angle[W(a_i, \tau)] = \phi(\tau) \tag{A4}$$

Instantaneous frequency of a signal in this case can be expressed as[21]

$$\omega(\tau) = \phi'(\tau) = \frac{1}{2\pi} \frac{d}{d\tau} (\angle[W(a_i, \tau)]) \quad (A5)$$

This shows that a general time-varying envelope $k(t)$ or phase $\phi(t)$ of the signal can be determined from the modulus and phase of the Morlet WT for each fixed wavelet frequency.

More specifically, from the impulse response of a single-degree-of-freedom viscous damper

$$x(t) = A \exp[-\zeta\omega_n t] \cos(\omega_d t + \phi_0) \quad (A6)$$

we can derive the following expressions from the WT of $x(t)$:

$$k(t) = \frac{|W(a_i, \tau)|}{\sqrt{a_i} \exp\left[-(a_i\omega(\tau) - \omega_0)^2\right]} = A \exp[-\zeta\omega_n t] \quad (A7)$$

$$\phi(t) = \angle[W(a_i, \tau)] = \omega_d t + \phi_0 \quad (A8)$$

For a constant wavelet frequency line corresponding to $a_i$ over time $\tau$ in the $(a, \tau)$ plane, estimation of the WT linear phase variation [or mean value of the instantaneous frequency, $\omega(t)$, over time] gives $\omega(t) \approx \omega_d$, and the envelope decay rate is $\zeta\omega_n$. Natural frequency $\omega_n$ and modal damping ratio $\zeta$ are, therefore, derived. The WT becomes a complex representation of the original real signal from which the signal eigenvalues are computed without any approximation of their range.

Multiple-degree-of-freedom systems are analyzed similarly by noting that the dilated Morlet wavelet is a bandpass filter. Instantaneous frequencies of several spectral components are resolved by separating them with a Morlet wavelet filter bank.[21] With sufficient resolution of dilation $a_i$, damped modal frequencies $\omega_{d_i} = \omega_0/a_i$ can be discriminated. To recap, the decay rate of the envelope of each mode is calculated from the log-slope of the wavelet modulus decay, and damped modal frequency is estimated as the linear phase variation of the WT as a function of time. Adequate frequency resolution can be enforced with the multiscaled compact harmonic Morlet wavelets.

# References

[1]Brenner, M. J., Lind, R. C., and Voracek, D. F., "Overview of Recent Flight Flutter Testing Research at NASA Dryden," AIAA Paper 97-1023, April 1997.

[2]Lind, R., Brenner, M., and Haley, S., "Estimation of Modal Parameters Using a Wavelet-Based Approach," AIAA Paper 97-3836, Aug. 1997.

[3]Freudinger, L. C., Lind, R., and Brenner, M. J., "Correlation Filtering of Modal Dynamics Using the Laplace Wavelet," *Proceedings of the 15th International Modal Analysis Conference*, Society for Experimental Mechanics, Inc., Bethel, CT, 1998, pp. 868–877.

[4]Atalla, M. J., "On Using the Wavelet Transform to Update Models," *Proceedings of the 16th International Modal Analysis Conference*, Society of Experimental Mechanics, Inc., Santa Barbara, CA, 1998, pp. 1675–1681.

[5]Ruzzene, M., Fasana, A., Garibaldi, L., and Piombo, B., "Natural Frequencies and Dampings Identification Using Wavelet Transform: Application to Real Data," *Mechanical Systems and Signal Processing*, Vol. 11, No. 2, 1997, pp. 207–218.

[6]Brenner, M. J., and Feron, E., "Wavelet Analysis of F/A-18 Aeroelastic and Aeroservoelastic Flight Test Data," AIAA Paper 97-1216, April 1997.

[7]Feron, E., Brenner, M., Paduano, J., and Turevskiy, A., "Time-Frequency Analysis for Transfer Function Estimation and Application to Flutter Clearance," *Journal of Guidance, Control, and Dynamics*, Vol. 21, No. 3, 1998, pp. 375–382.

[8]Xia, X.-G., "System Identification Using Chirp Signals and Time-Variant Filters in the Joint Time-Frequency Domain," *IEEE Transactions on Signal Processing*, Vol. 45, No. 8, 1997, pp. 2072–2084.

[9]Le, D. K., "Multiscale System Identification and Estimation" *SPIE Proceedings of Advanced Signal Processing Algorithms*, Society of Photo-Optical Instrumentation Engineers, Bellingham, WA, Vol. 2563, 1995, pp. 470–481.

[10]Le, D. K., "Application of Sampling Theorems in Wavelet Spaces to Multiresolution Visualization and Data Segmentation," *SPIE Proceedings of Wavelet Applications in Signal and Image Processing III*, Society of Photo-Optical Instrumentation Engineers, Bellingham, WA, Vol. 2569, 1995, pp. 220–233.

[11]Le, D. K., Owen, A. K., and Mattern, D. L., "Multiscale Analysis of Stall Inception and Instabilities in an Axi-Centrifugal Turboshaft Engine," AIAA Paper 96-3174, July 1996.

[12]Bowers, A. H., Pahle, J. W., Wilson, J. R., Flick, B. C., and Rood, R. L., "An Overview of the NASA F-18 High Alpha Research Vehicle," NASA TM-4772, Oct. 1996.

[13]Lind, R., and Brenner, M. J., "Robust Flutter Margin Analysis That Incorporates Flight Data," NASA TP-1998-206543, March 1998.

[14]Pahle, J. W., Powers, B., Regenie, V., Chacon, V., Degroote, S., and Murnyack, S., "Research Flight Control System Development for the F-18 High Alpha Research Vehicle," NASA TM-104232, 1991.

[15]Brenner, M. J., "Aeroservoelastic Modeling and Validation of a Thrust-Vectoring F/A-18 Aircraft," NASA TP-3647, Sept. 1996.

[16]Mallat, S., and Zhang, Z., "Matching Pursuit with Time-Frequency Dictionaries," *IEEE Transactions on Signal Processing*, Vol. 41, No. 12, 1993, pp. 3397–3415.

[17]Newland, D. E., *An Introduction to Random Vibrations, Spectral and Wavelet Analysis*, 3rd ed., Addison Wesley Longman, Boston, MA, 1993.

[18]Shensa, M. J., "Discrete Inverses for Nonorthogonal Wavelet Transforms," *IEEE Transactions on Signal Processing*, Vol. 44, No. 4, 1996, pp. 798–807.

[19]Shensa, M. J., "The Discrete Wavelet Transform: Wedding the À Trous and Mallat Algorithms," *IEEE Transactions on Signal Processing*, Vol. 40, No. 10, 1992, pp. 2464–2482.

[20]Meyer, Y., *Wavelets: Algorithms and Applications*, translated and revised by Robert D. Ryan, Society for Industrial and Applied Mathematics, Philadelphia, PA, 1993, pp. 63–73.

[21]Mallat, S., *A Wavelet Tour of Signal Processing*, Academic, 1998, pp. 64–126.

[22]Lind, R., and Brenner, M., "Analysis of Aeroservoelastic Stability Margins Using the $\mu$ Method," AIAA Paper 98-1895, April 1998.

[23]Packard, A., and Doyle, J., "The Complex Structured Singular Value," *Automatica*, Vol. 29, No. 1, 1993, pp. 71–109.

[24]Lind, R., and Brenner, M., "Incorporating Flight Data into a Robust Aeroelastic Model," *Journals of Aircraft*, Vol. 35, No. 3, 1998, pp. 470–477.

[25]Lind, R., and Brenner, M., "Robust Flutter Margins of an F/A-18 Aircraft from Aeroelastic Flight Data," *Journal of Guidance, Control, and Dynamics*, Vol. 20, No. 3, 1997, pp. 597–604.

[26]Lind, R. C., and Brenner, M. J., "A Worst-Case Approach for On-Line Flutter Prediction," 1997 CEAS International Forum on Aeroelasticity and Structural Dynamics, Rome, Italy, 1997, Vol. 2, pp. 79–86.